Polysaccharide hydrogels with tunable stiffness and provasculogenic properties via α-helix to β-sheet switch in secondary structure

Aurelien Forget[a,b], Jon Christensen[a,b], Steffen Lüdeke[c], Esther Kohler[a,b], Simon Tobias[a], Maziar Matloubi[a], Ralf Thomann[a], and V. Prasad Shastri[a,b,1]

[a]Institute for Macromolecular Chemistry, [b]BIOSS–Centre for Biological Signaling Studies, and [c]Institute for Pharmaceutical Sciences, University of Freiburg, 79104 Freiburg, Germany

Edited* by Robert Langer, Massachusetts Institute of Technology, Cambridge, MA, and approved July 1, 2013 (received for review January 2, 2013)

Mechanical aspects of the cellular environment can influence cell function, and in this context hydrogels can serve as an instructive matrix. Here we report that physicochemical properties of hydrogels derived from polysaccharides (agarose, κ-carrageenan) having an α-helical backbone can be tailored by inducing a switch in the secondary structure from α-helix to β-sheet through carboxylation. This enables the gel modulus to be tuned over four orders of magnitude (G′ 6 Pa–3.6 × 10^4 Pa) independently of polymer concentration and molecular weight. Using carboxylated agarose gels as a screening platform, we demonstrate that soft-carboxylated agarose provides a unique environment for the polarization of endothelial cells in the presence of soluble and bound signals, which notably does not occur in fibrin and collagen gels. Furthermore, endothelial cells organize into freestanding lumens over 100 μm in length. The finding that a biomaterial can modulate soluble and bound signals provides impetus for exploring mechanobiology paradigms in regenerative therapies.

extracellular matrix | vascular biology | angiogenesis | cell carrier | regenerative medicine

The organization of cells into tissue-like structures involves a complex interplay between soluble signals and those originating from the extracellular matrix (ECM). In recent years several studies have shown that cells can respond to physical cues (substrate stiffness and nanoroughness) in a very well-defined manner, and this may constitute another form of signaling (1–3). Mechanobiology—the interplay between biological and physical signals in establishing cell function—constitutes a new avenue for deciphering the signaling environment during tissue morphogenesis. In this regard, there is a need to develop systems that can enable the investigation and translation of mechanobiology paradigms into regenerative medicine solutions in vivo (4–6). Such a system has to meet the following criteria: offer precise tailoring of the mechanical environment in vivo, be cytocompatible, enable predictable evolution of cellular function, and exhibit human biocompatibility. Hydrogels, by virtue of their ability to mimic several aspects of physiological environments such as hydration state and interconnected pore architecture, have been explored extensively in this context as mimics of ECM (4) and in the de novo development of tissue (7–9). Hydrogels can be formed from either synthetic or natural water-soluble polymers, and the transformation of the polymer network into a gel requires the introduction of cross-links (net points) between polymer chains. Hydrogels of polyethylene glycol (PEG) and hyaluronic acid (HA), an ECM component, constitute the most prominent class of hydrogels for regenerative medicine applications, and they are formed through chemical [radical (acrylate) (10), Michael addition (vinyl sulfone) (11), or click chemistry (thiolene) (12)] or enzymatic (transglutaminase) cross-linking (13). In addition to HA, other polysaccharides such as alginate (14), which undergoes calcium-induced gelation (15, 16), and chitin (17) have also been explored. More recently, self-assembled peptides have emerged as yet another class of biologically derived hydrogels (18, 19).

To use hydrogels as instructive materials in the context of mechanobiology, precise control over the mechanics and biology within the hydrogel is essential. In a chemically cross-linked system varying the modulus necessitates changing the polymer concentration and/or polymer chain length. Additionally, implementation of chemical cross-linking in vivo can be challenging as it requires initiators and chemistries, which can also react with ECM components and proteins, and when not consumed can lead to toxicity. Agarose, a polysaccharide extracted from marine red algae composed of D-galactose-3,6-anhydro-L-galactopyranose repeat units, has received considerable attention in regenerative medicine in recent years due to its cytocompatibility, tissue compatibility in humans (20, 21), and ability to induce in vivo, the de novo formation of hyaline-like cartilage (8) and is currently undergoing phase-3 clinical trials in humans as a carrier for chondrocytes (22). Unlike PEG, HA, and alginate, agarose forms a hydrogel through physical cross-linking (23), which in comparison with chemical and ionic cross-linking offers several advantages including the absence of reactive chemistry and ease of implementation. However, manipulation of properties of a physically cross-linked system is challenging as increasing the polymer concentration beyond the gelation concentration yields only modest changes in stiffness, as in the case of agarose gels where increasing the concentration from 1% to 4% wt/vol increases the G′ by only sixfold (G′, 1.3 × 10^4 to 7.4 × 10^4 Pa). Therefore, new mechanisms for promoting association of polymer chains in physical gelation are needed.

Results and Discussion

Backbone Modification Diminishes Helical–Helical Interactions. Polysaccharides whose backbones are organized into α-helices such as agarose and κ-carrageenan can undergo thermally reversible gelation from aqueous solutions. The key step in their physical gelation is the aggregation of the double-stranded α-helices (24, 25). It has been reported that oxidation of the D-galactose primary alcohol residue in agarose results in weaker gels (26). We theorized that introduction of charged moieties such as carboxylic acid groups might impose strains on the polysaccharide backbone and that this could potentially alter helical interactions. To test this premise, molecular dynamics (MD) simulation in explicit water solvent was carried out on double-stranded dimers of the agarose repeat unit D-galactose-3,6-anhydro-L-galactopyranose with carboxylic acid modification (carboxylated agarose, CA) and without a carboxylic acid modification (native agarose, NA) in the C6 position. The starting conformation of the chains was defined

Author contributions: A.F., J.C., and V.P.S. designed research; A.F., J.C., E.K., S.T., M.M., and R.T. performed research; A.F., J.C., S.L., and V.P.S. analyzed data; and A.F., J.C., S.L., and V.P.S. wrote the paper.

The authors declare no conflict of interest.

*This Direct Submission article had a prearranged editor.

Freely available online through the PNAS open access option.

[1]To whom correspondence should be addressed. E-mail: prasad.shastri@gmail.com.

This article contains supporting information online at www.pnas.org/lookup/suppl/doi:10.1073/pnas.1222880110/-/DCSupplemental.

on the basis of the crystal structure of agarose and fiber X-ray diffraction data reported for the agarose double helix (24). Although a double α-helical conformation was imposed on both systems at the start of the simulation (Fig. S1), 8 ns into the simulation the CA strands started to move apart whereas the NA strands continued to remain in contact (Fig. 1*A*). At the end of the simulation (12 ns) the CA strands exhibited no interaction with one another whereas the NA strands were, as expected, intertwined into a double-stranded helix (Fig. 1*B*). The formation of double-stranded helices in proteins and oligonucleotides is driven by the ability of the macromolecular chains to form weak interactions through H bonds. It would therefore be reasonable to assume that the potential for the formation of such interactions would be a function of the distance between the H atoms and the electronegative oxygen (alcohol or carboxylic acid). Because carboxylation promotes separation of the polymer chains, this should also diminish the likelihood of H-bonding interactions. The analysis of the frequency of H bonds on a per frame basis over the entire simulation revealed that carboxylation indeed decreases the propensity of at least one H-bond formation by over 75% compared with NA (Fig. 1*C*) and furthermore the formation of no (zero) H bonds is almost doubled for CA vs. NA. These observations taken in sum hinted at the possibility that the introduction of a charged carboxylic acid group could potentially alter the associative behavior of the agarose helices.

Carboxylation Promotes a β-Sheet Secondary Structure. One potential outcome of introducing charges along a polymer backbone would be a transition of the polymer chains from a coiled morphology to a more extended morphology due to increased electrostatic repulsion between the chains (27). A technique commonly used to study secondary structure in biological molecules is circular dichroism (CD) (28). CD is very sensitive toward changes in the coupling of transition dipole moments, which serves as a probe for secondary structure, e.g., α-helices or β-sheets in proteins (28). In NA the CD arises from coupling of C-O-C ether chromophores, leading to positive residual ellipticity with a maximum at 183 nm for α-helices (Fig. 2*A*) (29). This ellipticity can be directly attributed to the α-helices, as it is absent in oligomeric agarose obtained from acid-catalyzed hydrolysis, which is incapable of organizing into an α-helix (Fig. S2*A*). To study potential changes to the agarose secondary structure upon carboxylation (Fig. S3), 93% carboxylated agarose (93-CA) was used as a model system. Like NA, 93-CA exhibits strong positive ellipticity; however, in comparison with NA the maximum is even stronger and red-shifted (191 nm) (Fig. 2*A*) and, additionally, the red shift is accompanied by the emergence of a new peak at 203 nm. The new ellipticity at 203 nm can be attributed to the carboxylation of the backbone, as its maximum increases exponentially with carboxylation (Fig. 2*B*). The change in molar absorptivity and shift to a lower energy excitation wavelength of the primary ellipticity may also be due to chromophore contributions of the introduced carboxyl group to the network of dipolar couplings in the α-helices in 93-CA. It therefore appears that the modification of the NA backbone promotes a reorganization of the chains leading to a new secondary structure in CA in addition to the native α-helices. In protein CD spectra positive ellipticity around 217 nm indicates β-sheets (28). Likewise, the secondary structure-related ellipticity at 203 nm in the CD spectrum of 93-CA may be attributed to a β-sheet–like conformation of the polysaccharide chains. Further evidence for the molecular reorganization leading to a new secondary structure was obtained by analyzing the MD simulation data. In proteins, the occurrence of helical or β-sheet motifs can be determined using the empirical Ramachandran plot (30). Extending this approach to polysaccharides (31), the empirical distributions of the dihedral angles ϕ and ψ of the glycosidic backbone (Fig. S2*B*) were plotted (Fig. 2*C*). As expected, in the case of NA the Ramachandran plot reveals the predominance of helical conformation. However, in contrast the coordinates of the CA dihedrals are mainly located in the β-sheet region consistent with the CD spectra, and this implies a dramatic reorganization of the polysaccharide backbone upon carboxylation. Such an α-helix to β-sheet transformation, although reported in proteins, is highly restricted but has not been observed before in polysaccharides.

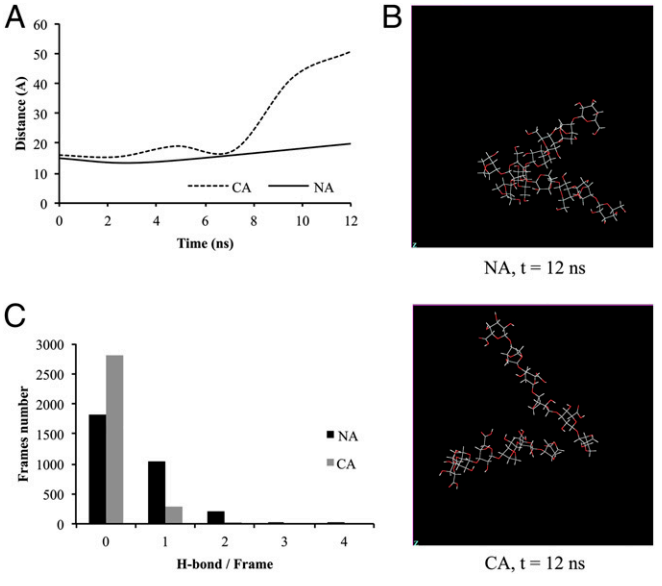

Fig. 1. Backbone modification diminishes helical–helical interactions. (*A*) A plot of average distance in angstroms between two strands of NA and CA, as determined by the distance between the glycosidic ether oxygens of the two strands in the MD simulation. (*B*) Snapshot of the MD simulation at t =12 ns for NA (*Upper*) and CA (*Lower*). (*C*) A plot of the frequency of the number of potential H bonds per frame for NA and CA as determined from MD simulations.

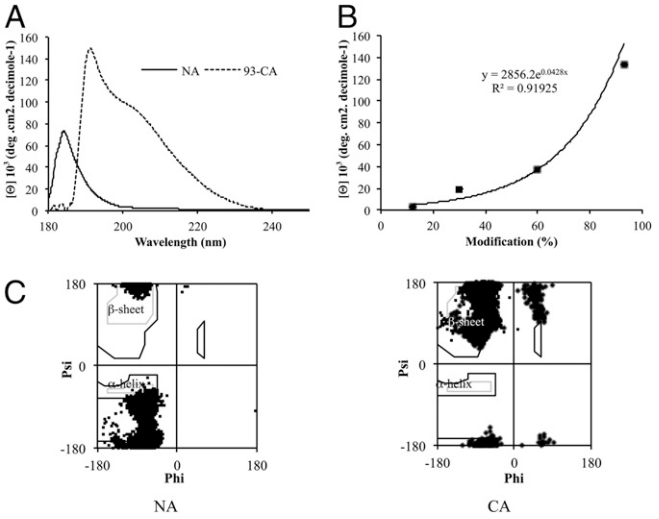

Fig. 2. Carboxylation promotes a β-sheet secondary structure. (*A*) CD spectrum of a 0.15% wt/vol solution of NA and 60-CA obtained below the T_{gel}. (*B*) Plot of the ellipticity at 203 nm as a function of carboxylation. Solution concentration is 0.15% wt/vol. In native agarose 12% of the C6 primary alcohol is not accessible for oxidation due to methylation (23). (*C*) Ramachandran plot of NA (*Left*) and CA (*Right*).

β-Sheet Secondary Structure Influences Chain Organization, Microstructure, and Gelation. To ascertain the impact of the β-sheet structure on the organization of agarose molecules, tapping mode atomic force microscopy (AFM) (32) was used to visualize NA and CA molecules (Fig. 3*A*). It is clear that the NA strands are organized as helical structures (Fig. 3*A*, *Inset*), appearing like "a string of pearls"

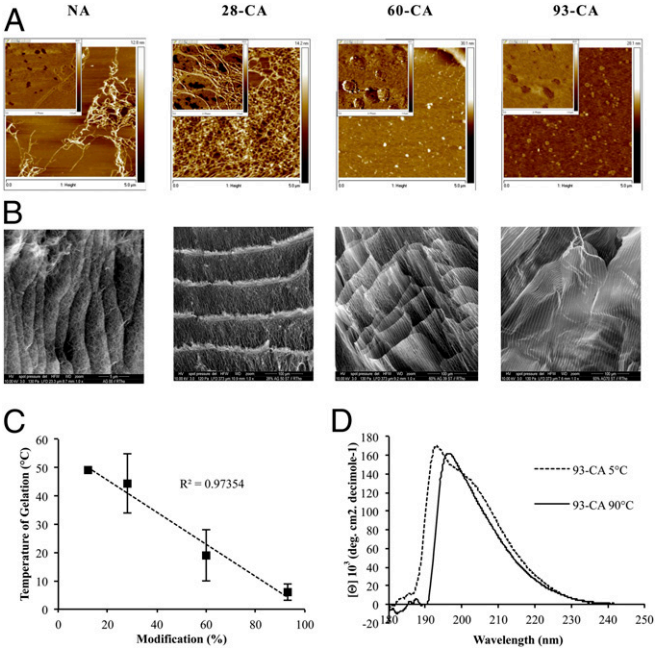

Fig. 3. β-Sheet structure influences chain organization, microstructure, and gelation. (*A*) Tapping mode AFM of single-molecule height (main plot) and phase (*Inset*) for NA and CA. (*B*) ESEMs of freeze-dried 2% wt/vol hydrogel of NA and CA. (*C*) Gelation temperature as a function of degree of carboxylation. This was determined on 2% wt/vol hydrogels of NA and CA by following G′ and G″ as a function of temperature. (*D*) CD spectrum of 0.15% wt/vol solution of 93-CA below T_{gel} (5 °C) and above T_{gel} (90 °C).

(Fig. 3*A*, *Left*). At 28% carboxylation (28-CA), the helical organization appears slightly disrupted and this is consistent with the CD data for 28-CA, where only a small shoulder associated with the ellipticity at 203 nm is observed. However, increasing carboxylation (60%, 60-CA; and 93%, 93-CA) results in the complete reorganization of fibers into disk-shaped structures that appear to have some residual helical motifs. Interestingly, fibers of soluble amyloid-β (Aβ), peptide fibrils that possess mixed β-sheet structures, also form circular globules, like those observed in the 60-CA and the 93-CA (33, 34). Because the molecular mass of agarose after oxidation [M_n, 88–94 kDa; polydispersity index (PDI), 2.14–2.23] is virtually identical to that of NA (M_n, 95 kDa; PDI, 2.99–3.12) (Fig. S4*A*), its contribution to the observed structural changes can be ruled out. The visual evidence is compelling and consistent with the CD data and the Ramachandran plot predictions, and they all point to the presence of a unique secondary structure in CA. Although the exact mechanism that drives the molecular reorganization of helix into β-sheet is not fully understood, one could postulate a prominent role for reduced H bonding and increased electrostatic repulsion between chains upon carboxylation, which, in sum, may promote more hydrophobic interactions leading to hitherto unknown interactions between agarose molecules.

In proteins, changes to secondary structure can alter protein folding (tertiary structure) in a manner that favors aggregation. In fact, soluble Aβ has a disordered structure; however, aggregates of Aβ have a significant amount of β-sheet structure (35). If the paradigm for structure evolution is conserved between polysaccharides and proteins, then one might expect that the switch from α-helix to β-sheet could also impact the supramolecular assembly of the agarose molecules and hence the microstructure of the gel. To determine whether this indeed occurs and to what extent, the interior of freeze-dried 2% wt/vol hydrogels was characterized using environmental scanning electron microscopy (ESEM). Whereas the microstructure of the NA gel was composed of tufts of disordered fibers, microstructures of the CA gel bear no resemblance to NA and reveal an astonishing transformation in the organization of agarose fibers, with increasing carboxylation (Fig. 3*B*). Even at a low degree of carboxylation (28%), the fibers are organized into ridge-like structures, composed of high-aspect ratio cells that appear to have some periodicity. Increasing the carboxylation to 60% further enhanced this organization, wherein disk-shaped motifs appear to fuse to one another in columnar strands organized into lamellae. At 93% carboxylation, the fiber organization appears to have undergone a fundamental change, resulting in sheet-like structures composed of highly oriented ribbons. Because 93-CA chains are organized into disk-shaped structures, their assembly into sheets would require an unraveling followed by lateral stacking. There is precedence for such a process in the literature. It has been shown that the transformation of Aβ42 disk-shaped oligomers into fibrils involves organization of the peptide strands within these oligomers into β-sheets (36). To the best of our knowledge, this is a unique report of the switching of the three-dimensional (3D) structure of a polymer hydrogel from a random organization of fibers to a lamellar structure.

As described earlier, the gelation of NA involves association of α-helices through H bonding mediated by the C6 primary hydroxyl group. Because carboxylation modifies helical interactions, it may also impose changes to the physicochemical characteristics of CA gels. The gelation behavior of agarose shows a hysteresis in that the melting temperature of the gel (T_m, >80 °C) is significantly higher than the gelation temperature (T_{gel} ~ 40 °C) (23). This is expected, as the formation of the gel requires H bonding, which is more likely to occur as the entropy of the system is reduced. A key prediction of the MD simulation is that CA chains have markedly diminished associative tendencies, resulting in lower H-bond formation (Fig. S4*B*). One implication of this prediction is lowering of the gelation temperature, as promotion of H bonding would require lower kinetic energy. In fact, the complete carboxylation of agarose results in the lowering of the T_{gel} to below 10 °C (i.e., $\delta = -30$ °C) over agarose, with intermediate carboxylation yielding intermediate T_{gel} (Fig. 3*C* and Fig. S5*A*). The lower gelation temperature is highly desirable for cell encapsulation and tissue regeneration applications, as activation of heat-shock proteins can be avoided (37). Concrete proof for the direct involvement of the β-sheet in the gelation of the CA gels was obtained by following the CD spectrum of 93-CA (fully carboxylated agarose) as a function of temperature. The CD spectrum of the 93-CA gel above its T_m shows a complete abolishment of the ellipticity at 203 nm associated with the β-sheet structure and additionally a further red shift of the ellipticity at 199 nm in comparison with the gel at 5 °C (Fig. 3*D*). This provides strong evidence that in CA the new β-sheet organization is responsible not only for the physical cross-linking of the gel but also for the dominant associative interaction between the polysaccharide chains.

Mechanism of Gelation of CA. On the basis of the observations at hand a mechanism for the gelation of CA is put forth involving the following four steps: (*i*) reorganization of the polymer backbone due to disruption of helices, resulting in α-helix to β-sheet switch; (*ii*) followed by aggregation of polymer chains through β-sheet motifs; (*iii*) elongation of these aggregates into high-aspect ratio structures; and (*iv*) the assembly of these high-aspect ratio structures in higher lamellar sheets (Fig. S6).

α-Helix to β-Sheet Reorganization of the Polymer Backbone Enables Tailoring of Modulus of Gels. Cross-links are often described as knots or entanglements of two and more chains. Because the gelation in both NA and CA can be attributed to association of secondary structure of a specific conformation, the cross-links can be imagined as assimilation of these secondary structures into soft spheres, and its formation can be likened to the growth of nanoparticles through phase inversion. These highly specific associative processes can manifest in dilute solutions as aggregates. The size, polydispersity (PD), and zeta potential (ζ) of aggregates that are spontaneously formed in dilute solutions of NA and CA were determined using dynamic light scattering. The average size of aggregates

formed in NA solution (0.15% wt/vol) was 1.09 μm, with a PD of ~0.6, suggesting a rather heterogeneous associative process. In contrast, the aggregates formed from CA solutions were almost half the size, around 600 nm, and more narrowly dispersed (PD ~ 0.3), implying a higher homogeneity (Fig. S7*A*). In fact, the changes to the size of the cross-links manifest themselves as a loss of turbidity in the gels, which is concomitant with increased carboxylation (Fig. S7*B*).

Assuming that these aggregates represent the origins of physical cross-linking, then their charge characteristics will influence their crystallization into a gel network. Although aggregates of NA have only a slightly negative ζ (−5 mV), ζ of the CA aggregate becomes increasingly negative (maximum −27 mV, Fig. S7*C*). On the basis of the colloidal crystallization theory one would expect that increasing surface charge would favor a more highly organized structure (38) but a much looser association due to electrostatic repulsion (39), thereby resulting in gels with a very well-defined microstructure, but that are physically weaker. Rheology studies reveal that this is indeed the case, with CA gels having lower G′ and G″ in comparison with NA. A typical rheology curve of storage (G′) and loss (G″) modulus as a function of angular frequency for NA and 60-CA is shown in Fig. 4*A*. The reduction in G′ is consistent with the predictions from the MD simulations, as a lower tendency for H bonding (Fig. S4*B*) coupled with an increased charged density along the polysaccharide should lower friction at the molecular level, thereby reducing the shear modulus of the gel (39). More importantly, by varying the degree of carboxylation, the G′ of gels can be tailored independent of the polysaccharide concentration, for example for a 2% wt/vol gel over four orders of magnitude (from 3.6×10^4 Pa to 6 Pa), spanning the entire range of soft tissues found in the mammalian anatomy (40), and over a slightly reduced range of G′ for a 4% wt/vol gel (Fig. 4*B*). The origin of the changes to G′ can be exclusively attributed to the new secondary structure as both NA and CA have identical molecular weights and PDI (Fig. S4*A*).

Carboxylation—A General Strategy for Transformation of Secondary Structure of Helical Polysaccharides. The ability to influence secondary structure of polysaccharides via carboxylation is not limited to agarose but can also be demonstrated in κ-carrageenan, a polysaccharide that, like agarose, also organizes into helical structures. Carboxylation of the primary alcohol at C6 position of sulfated D-galactose in κ-carrageenan results in changes to the CD spectrum that are identical to those in agarose (Fig. S8*A*). Upon carboxylation, the negative residual ellipticity of κ-carrageenan β-helices undergoes a red shift from 183 nm to 189 nm, which is again accompanied by a new residual ellipticity with a maximum at 203 nm. The opposite sign of these two spectral features clearly demonstrates the coexistence of two secondary structural elements, β-helix and β-sheet, in a single polysaccharide. Furthermore, AFM images reveal that carboxylation of κ-carrageenan promotes the transition of polymer fibers from helical to disk-shaped assemblies as observed in CA (Fig. S8*B*). Even more remarkable is that the switch from helices to β-sheets, like in the case of agarose, induces reorganization of the microstructure of the freeze-dried gels from fibrous (unmodified κ-carrageenan, KC) to a high-ordered lamellar structure (carboxylated κ-carrageenan, CKC) (Fig. S8*C*). If the organization of polymer fibers in carboxylated κ-carrageenan is indeed driven by the association of β-sheets, like in CA, then one would predict a lower modulus for carboxylated κ-carrageenan in comparison with κ-carrageenan. Indeed, the G′ for carboxylated κ-carrageenan is three orders of magnitude lower than that for κ-carrageenan (Fig. S8*D*). On the basis of these observations, this result might provide a general approach for altering secondary structure α-helical polysaccharides.

CA60 Gels Promote Human Umbilical Vein Endothelial Cell Organization into Lumens. The organization of cells into tissue-like structures involves a complex interplay between the soluble signals and those originating from the ECM (matrix stiffness, cell–ECM binding motifs, bound growth factors). Because stiffness of a biomaterial has been shown to impact stem cell lineage choices (1) and the metastasis of cancer cells (41), we envisage that these injectable CA gels with tunable mechanical and structural properties would be highly desirable for cell delivery and as a clinically translatable system for controlled tissue morphogenesis.

Vascularization is critical for the survival of cells and necessary for the transport of signaling molecules to aid in regeneration. Vasculogenesis, as it pertains to in vitro studies, is the formation of lumens from dispersed endothelial cells (ECs), and it differs from angiogenesis where ECs sprout from an existing blood vessel or an EC monolayer (42). It is well established that during vascular lumen morphogenesis, i.e., the formation of arteriole-like structures, cell–cell contacts and mural (support) cells play a vital role. To identify the factors that influence EC organization, several in vitro models have been established, including collagen gel, fibrin gel, and matrigel (43–46). These studies have revealed that arginine–glycine–aspartic acid (RGD) integrin binding sequence and soluble signals such as vascular endothelial growth factor (VEGF) and fibroblast growth factor-2 (FGF-2) are essential and that the mechanical aspects of the gel impact the formation of EC networks (43–46). Nevertheless, the factors that impact the organization of multiple ECs in freestanding tubular structures are not fully understood. Because vasculogenesis primarily occurs during embryonic development when ECM is immature, we attempted to recreate matrix and cues representing early development by screening the impact of the gel modulus and bound and soluble signals on human umbilical vein endothelial cell (HUVEC) organization. Our hypothesis was that the immediate cellular environment must have a critical role in how soluble and bound signals are perceived by ECs. To investigate this premise further we studied the organization of HUVECs in CA gels of two moduli, 0.02 kPa (CA60) and 1 kPa (CA28), by systematically altering three parameters: basement membrane proteins (±0.01% wt/vol Matrigel), cell-binding motif (±RGD) (Fig. S5 *B* and *C*), and soluble signals [±VEGF, FGF, and Phorbol 12-myristate 13-acetate (PMA)] (Table S1). In comparison, HUVECs were also cultured in fibrin gel and collagen gel supplemented with 0.01% Matrigel and soluble signals and in Matrigel supplemented with soluble signals.

The organization of HUVECs into lumens can be categorized into four types as shown in Fig. 5*A*. Phase contrast images of HUVECs in the various gel environments are shown in Fig. S9. In general, the organization of HUVECs in fibrin and collagen gels involved one to two cells and exhibited characteristics of type I and type II lumens (Fig. 5*B*). However, in contrast, HUVECs in

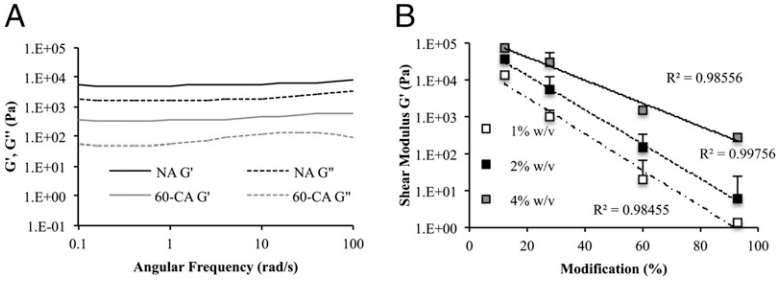

Fig. 4. α-Helix to β-sheet reorganization of the polymer backbone enables tailoring of modulus of gels. (*A*) Comparison of rheological behavior of NA and 60-CA. Carboxylation results in the reduction of both shear (G′) and storage (G″) modulus. (*B*) G′ as a function of degree of carboxylation and polymer concentration. G′ in CA can be tailored over four orders of magnitude independently of polymer concentration.

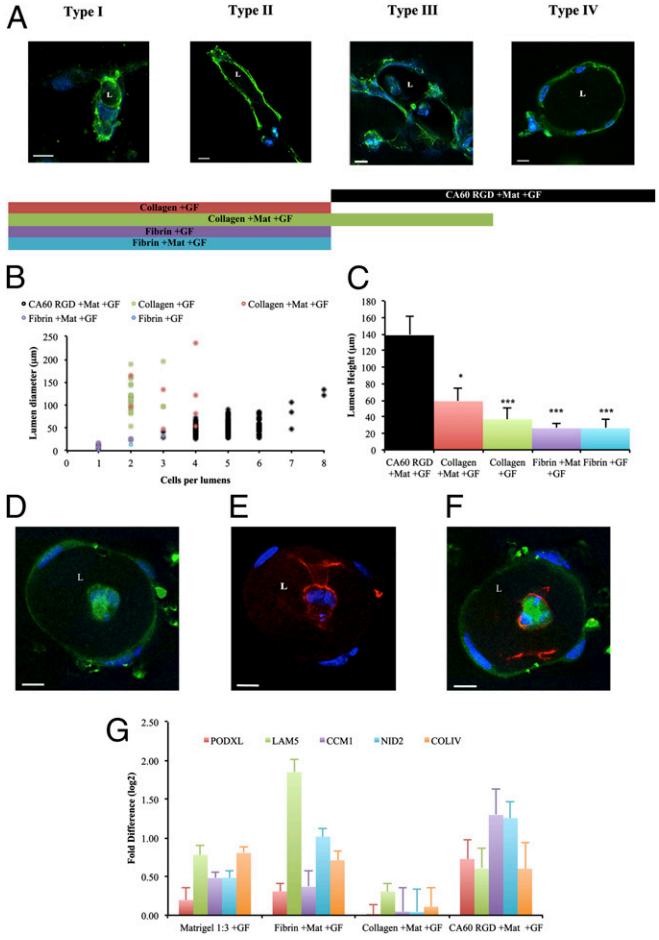

Fig. 5. Carboxylated agarose gels are provasculogenic in vitro. (*A*) HUVEC lumen morphology in gels. The organization of HUVECs into 2D lumens (L) can be categorized into four types: oval structures composed of a single cell, type I; elliptical structures composed of two cells, type II; circular structures composed of two to four cells, type III; and circular structures composed of more than four cells, type IV. Blue, DAPI nuclear stain; green, F-Actin. (Scale bar: 10 μm.) The color-coded bars at the bottom span morphologies typically observed under the various conditions. (*B*) Scatter plot of diameter and cell numbers associated with lumens. It is clear that the lumens observed in CA60 gels supplemented with Matrigel and GF are primarily composed of more than four cells and 50–100 μm in diameter. Note that data points from fibrin gel under both conditions (+GF and +Matrigel/+GF) overlap significantly. (*C*) Large-scale organization of HUVECs. HUVECs are organized into lumens over 100 μm in height in CA68 gels. This represented a >50% increase in comparison with collagen (+Matrigel/+GF and +GF) and over an order of magnitude greater in comparison with fibrin. Asterisks represent statistical significance compared with CA60 gel (*P < 0.05, ***P < 0.001). (*D*–*F*) Apical–basal polarization of HUVECs in CA60 gels. Visualization of human PODXL and COL4 was carried out using fluorescent immunohistochemisty: COL4 (green) (*D*), PODXL (red) (*E*), merged image (*F*). Blue, DAPI nuclear stain. (Scale bar, 10 μm.) (*G*) mRNA expression level of key provasculogenic markers in HUVECs. The expression of PODXL and NID2 in HUVECs in CA60 gels supplemented with Matrigel/GF was notably higher than expression of those in fibrin and collagen gels supplemented with Matrigel/GF and Matrigel supplemented with GF. This is consistent with the ability of HUVECs to undergo apical–basal polarization in CA60 gels. (Scale bar: 10 μm.)

CA60 modified with RGD and supplemented with basement membrane proteins and soluble signals showed type III and type IV structures, with more than three HUVECs participating in the formation of the lumens (Fig. 5*B*). Interestingly, no such organization was observed in the CA60 gels in the absence of RGD, basement membrane proteins, and soluble factors (Table S1). Analysis of the frequency and structural characteristics (diameter and length) of the lumens revealed significant differences. In general more lumens were observed in CA60 gels in comparison with both fibrin and collagen gels (Fig. 5*B*). Furthermore, despite higher cell numbers per lumen the diameters of lumens formed in the CA60 gels were quite homogeneous at around 50–100 μm. However, more heterogeneity was observed in collagen and fibrin gels (Fig. 5*B*). Another significant observation was that HUVECs in CA60 gels could organize into freestanding, hollow, tubular structures over 100 μm in length, resembling arterioles (Fig. 5*C*, Fig. S10 slices, and Movie S1). In contrast, the average length of such structures was about 50% smaller in collagen gels and an order of magnitude lower in fibrin gels (Fig. 5*C* and Figs. S11–S13). This maybe attributed to the observed differences in the polarization potential of HUVECs as discussed below.

HUVECs Undergo Polarization in CA60 Gels. Apical–basal polarization of ECs is a critical step in the formation of stable blood vessels (47). Immunofluorescent staining against human podocalyxin (PODXL) and type-4 collagen (COL4A1) revealed apical and basal localization of PODXL and COL4A1, respectively, in HUVECs in CA60 gels, suggesting that they had undergone apical–basal polarization (Fig. 5 *D* and *E*). In comparison, HUVECs in fibrin and collagen gels did not stain for human PODXL and COL4A1. This is consistent with the down-regulation at the mRNA level of PODXL and NID2, both of which are necessary for lumen expansion and maturation, in both collagen and fibrin gels in comparison with CA60 (Fig. 5*G*). It is noteworthy that the lumens appear to originate from a cluster of HUVECs that are already polarized, i.e., show apical localization of PODXL. This is in accordance with literature reports that vascular lumen morphogenesis requires the polarization of an EC cluster (three to five cells), which involves the recruitment of PODXL at the apical surface, which then initiates lumen expansion (47). A factor that might contribute to the formation of HUVEC clusters is the superior proliferation of the HUVECs in the CA60-RGD–modified gel, which is twofold greater than under expansion conditions on tissue culture plastic (Fig. S14). Interestingly, the incorporation of basement membrane proteins, i.e., Matrigel, had no effect on lumen length in fibrin gels and provided only a marginal increase in collagen gels (Fig. 5*C*) and this was also consistent with the lack of appreciable changes to the expression of key vasculogenesis markers at the mRNA level (Table S2, Fig. S15*A*). This implies that the observed organization of HUVECs into lumens in CA60 gels cannot be attributed solely to the presence of growth factors and basement membrane proteins because HUVECs in Matrigel while staining positive for PODXL and COL4 do not shown apical/basal localization and also do not organize into lumens (Fig. S16). A noteworthy observation is that HUVECs in the CA28 gels, although showing comparable expression levels of the provasculogenic markers in comparison with HUVECs in CA60 gels at the mRNA level (Fig. S15*B*), however, remain dispersed and fail to organize (Fig. S9), thus suggesting a role for biophysical variables.

Several mechanisms might contribute to the provasculogenic characteristics of the low-modulus CA gels. In biological gels such as fibrin and collagen, proteolytic degradation of the matrix by membrane-type matrix metalloproteinases is necessary and critical, as it paves the way for the migration and organization of the ECs (43). Because CA cannot undergo proteolytic degradation, the role of matrix degradation in the organization of HUVECs in CA gels can be ruled out. However, it is possible that the stiffness and the chemistry of the gel can modulate the organization and affinity of ECM components and soluble signals. Because the stiffness of fibrin and collagen gels is similar to that of CA60 (Table S3), this suggests that the origin of the provasculogenic nature of CA60 may lie in its unique physicochemical properties (backbone charge and secondary structure) and not solely in its stiffness. Another aspect worth considering is the modulation of HUVEC function by the CA gel through a mechanobiology paradigm. This would require mechanical coupling between the gel matrix and the cell through the RGD

motif and a unique role for this motif in HUVEC function. It has long been recognized that RGD signaling is important for EC survival and proliferation (48). Furthermore, it is well known that β1-integrin signaling is important in arterial tubulogenesis and β1 integrins have a binding site for RGD (49). Therefore, it is conceivable that β1 integrins on the HUVECs (50) mechanically couple to the gel through the RGD ligand and thereby sense the mechanical environment provided by the gel. Interestingly, among 32 conditions screened, HUVEC organization into lumens occurs only in CA60 gels modified with RGD. On the basis of these findings, we conclude that CA gels are well suited for understanding and leveraging the role of mechanobiology in tissue morphogenesis and provide a potential translational platform for regenerative therapies.

Materials and Methods

For materials and methods used in this study, please see *SI Materials and Methods*.

ACKNOWLEDGMENTS. The authors thank Drs. Daniel Vonwil and Christopher Pino for valuable suggestions, Dr. Christian Friedrich for providing access to the rheology instrument, and Prof. Roland Nitschke for help with confocal imaging. This work was supported by the excellence initiative of the German Federal and State Governments Grant EXC 294 (Centre for Biological Signaling Studies) and the University of Freiburg.

1. Engler AJ, Sen S, Sweeney HL, Discher DE (2006) Matrix elasticity directs stem cell lineage specification. *Cell* 126(4):677–689.
2. Lipski AM, Pino CJ, Haselton FR, Chen I-W, Shastri VP (2008) The effect of silica nanoparticle-modified surfaces on cell morphology, cytoskeletal organization and function. *Biomaterials* 29(28):3836–3846.
3. Lutolf MP, Doyonnas R, Havenstrite K, Koleckar K, Blau HM (2009) Perturbation of single hematopoietic stem cell fates in artificial niches. *Integr Biol* 1(1):59–69.
4. Lutolf MP, Hubbell JA (2005) Synthetic biomaterials as instructive extracellular microenvironments for morphogenesis in tissue engineering. *Nat Biotechnol* 23(1): 47–55.
5. Shastri VP (2009) In vivo engineering of tissues: Biological considerations, challenges, strategies, and future directions. *Adv Mater* 21(32–33):3246–3254.
6. Shastri VP (2012) Delivering regeneration. *Drug Deliv Transl Res* 2:293–296.
7. Elisseeff J, et al. (1999) Transdermal photopolymerization for minimally invasive implantation. *Proc Natl Acad Sci USA* 96(6):3104–3107.
8. Emans PJ, et al. (2010) Autologous engineering of cartilage. *Proc Natl Acad Sci USA* 107(8):3418–3423.
9. Stevens MM, et al. (2005) In vivo engineering of organs: The bone bioreactor. *Proc Natl Acad Sci USA* 102(32):11450–11455.
10. Aimetti AA, Machen AJ, Anseth KS (2009) Poly(ethylene glycol) hydrogels formed by thiol-ene photopolymerization for enzyme-responsive protein delivery. *Biomaterials* 30(30):6048–6054.
11. Lutolf MP, Hubbell JA (2003) Synthesis and physicochemical characterization of end-linked poly(ethylene glycol)-co-peptide hydrogels formed by Michael-type addition. *Biomacromolecules* 4(3):713–722.
12. DeForest CA, Polizzotti BD, Anseth KS (2009) Sequential click reactions for synthesizing and patterning three-dimensional cell microenvironments. *Nat Mater* 8(8): 659–664.
13. Ehrbar M, et al. (2007) Enzymatic formation of modular cell-instructive fibrin analogs for tissue engineering. *Biomaterials* 28(26):3856–3866.
14. Augst AD, Kong HJ, Mooney DJ (2006) Alginate hydrogels as biomaterials. *Macromol Biosci* 6(8):623–633.
15. Huebsch N, et al. (2010) Harnessing traction-mediated manipulation of the cell/matrix interface to control stem-cell fate. *Nat Mater* 9(6):518–526.
16. Stevens MM, Qanadilo HF, Langer R, Prasad Shastri V (2004) A rapid-curing alginate gel system: Utility in periosteum-derived cartilage tissue engineering. *Biomaterials* 25(5):887–894.
17. Tamura H, Nagahama H, Tokura S (2006) Preparation of chitin hydrogel under mild conditions. *Cellulose* 13:357–364.
18. Hartgerink JD, Beniash E, Stupp SI (2002) Peptide-amphiphile nanofibers: A versatile scaffold for the preparation of self-assembling materials. *Proc Natl Acad Sci USA* 99(8):5133–5138.
19. Kopecek J, Yang J (2009) Peptide-directed self-assembly of hydrogels. *Acta Biomater* 5(3):805–816.
20. Fernández-Cossío S, León-Mateos A, Sampedro FG, Oreja MTC (2007) Biocompatibility of agarose gel as a dermal filler: Histologic evaluation of subcutaneous implants. *Plast Reconstr Surg* 120(5):1161–1169.
21. Selmi TA, Neyret P, Verdonk PCM, Barnouin L (2007) Autologous chondrocyte transplantation in combination with an alginate-agarose based hydrogel. *Tech Knee Surg* 6:253–258.
22. Selmi TA, et al. (2008) Autologous chondrocyte implantation in a novel alginate-agarose hydrogel: Outcome at two years. *J Bone Joint Surg Br* 90(5):597–604.
23. Lahaye M, Rochas C (1991) Chemical structure and physico-chemical properties of agar. *Hydrobiologia* 221(1):137–148.
24. Arnott S, et al. (1974) The agarose double helix and its function in agarose gel structure. *J Mol Biol* 90(2):269–284.
25. Djabourov M, Clark AH, Rowlands DW, Ross-Murphy SB (1989) Small-angle x-ray scattering characterization of agarose sols and gels. *Macromolecules* 22(1):180–188.
26. Cao X, Shoichet MS (2002) Photoimmobilization of biomolecules within a 3-dimensional hydrogel matrix. *J Biomater Sci Polym Ed* 13(6):623–636.
27. Myer YP (1969) The pH-induced helix-coil transition of poly-L-lysine and poly-L-glutamic acid and the 238-mu dichroic band. *Macromolecules* 1379:624–628.
28. Woody RW, Berova N, Polavarapu PL, Nakanishi K, eds (2012) *Comprehensive Chiroptical Spectroscopy* (Wiley, New York), pp 475–497.
29. Arndt ER, Stevens ES (1997) Anhydro sugar and linkage contributions to circular dichroism of agarose and carrageenan, with conformational implications. *Carbohydr Res* 303(1):73–78.
30. Ramachandran GN, Ramakrishnan C, Sasisekharan V (1963) Stereochemistry of polypeptide chain configurations. *J Mol Biol* 7:95–99.
31. Lütteke T, Frank M, von der Lieth C-W (2005) Carbohydrate Structure Suite (CSS): Analysis of carbohydrate 3D structures derived from the PDB. *Nucleic Acids Res* 33(Database issue):D242–D246.
32. Takahiro F (2010) Atomic force microscopy imaging of food polysaccharides. *Measurement* 16(1):1–12.
33. vandenAkker CC, Engel MFM, Velikov KP, Bonn M, Koenderink GH (2011) Morphology and persistence length of amyloid fibrils are correlated to peptide molecular structure. *J Am Chem Soc* 133(45):18030–18033.
34. Ganesh S, Jayakumar R (2003) Structural transitions involved in a novel amyloid-like beta-sheet assemblage of tripeptide derivatives. *Biopolymers* 70(3):336–345.
35. Blackley HK, et al. (2000) In-situ atomic force microscopy study of beta-amyloid fibrillization. *J Mol Biol* 298(5):833–840.
36. Ahmed M, et al. (2010) Structural conversion of neurotoxic amyloid-beta(1-42) oligomers to fibrils. *Nat Struct Mol Biol* 17(5):561–567.
37. Whitley D, Goldberg SP, Jordan WD (1999) Heat shock proteins: A review of the molecular chaperones. *J Vasc Surg* 29(4):748–751.
38. Rugge A, Tolbert SH (2002) Effect of electrostatic interactions on crystallization in binary colloidal films. *Langmuir* 18(18):7057–7065.
39. Okano T, Araki J, Masahisa W, Shigenori K (1999) Influence of surface charge on viscosity behavior of cellulose microcrystal suspension. *J Wood Sci* 45:258–261.
40. Reilly GC, Engler AJ (2010) Intrinsic extracellular matrix properties regulate stem cell differentiation. *J Biomech* 43(1):55–62.
41. Paszek MJ, et al. (2005) Tensional homeostasis and the malignant phenotype. *Cancer Cell* 8(3):241–254.
42. Vailhé B, Vittet D, Feige JJ (2001) In vitro models of vasculogenesis and angiogenesis. *Lab Invest* 81:439–452.
43. Lafleur MA, Handsley MM, Knäuper V, Murphy G, Edwards DR (2002) Endothelial tubulogenesis within fibrin gels specifically requires the activity of membrane-type-matrix metalloproteinases (MT-MMPs). *J Cell Sci* 115(Pt 17):3427–3438.
44. Sieminski AL, Hebbel RP, Gooch KJ (2004) The relative magnitudes of endothelial force generation and matrix stiffness modulate capillary morphogenesis in vitro. *Exp Cell Res* 297(2):574–584.
45. Koh W, Stratman AN, Sacharidou A, Davis GE (2008) In vitro three dimensional collagen matrix models of endothelial lumen formation during vasculogenesis and angiogenesis. *Methods Enzymol* 443:83–101.
46. Arnaoutova I, George J, Kleinman HK, Benton G (2009) The endothelial cell tube formation assay on basement membrane turns 20: State of the science and the art. *Angiogenesis* 12(3):267–274.
47. Herbert SP, Stainier DYR (2011) Molecular control of endothelial cell behaviour during blood vessel morphogenesis. *Nat Rev Mol Cell Biol* 12(9):551–564.
48. Oguey D, George PW, Rüegg C (2000) Disruption of integrin-dependent adhesion and survival of endothelial cells by recombinant adenovirus expressing isolated beta integrin cytoplasmic domains. *Gene Ther* 7(15):1292–1303.
49. Shiokawa S, et al. (1999) Functional role of arg-gly-asp (RGD)-binding sites on β1 integrin in embryo implantation using mouse blastocysts and human decidua. *Biol Reprod* 60(6):1468–1474.
50. Leavesley DI, Schwartz MA, Rosenfeld M, Cheresh DA (1993) Integrin beta 1- and beta 3-mediated endothelial cell migration is triggered through distinct signaling mechanisms. *J Cell Biol* 121(1):163–170.